Meteorol Atmos Phys (2010) 109:107–114
DOI 10.1007/s00703-010-0097-5

ORIGINAL PAPER

Torrential rainfall responses to radiative and microphysical processes of ice clouds during a landfall of severe tropical storm Bilis (2006)

Donghai Wang · Xiaofan Li · Wei-Kuo Tao

Received: 19 April 2010 / Accepted: 6 October 2010 / Published online: 24 October 2010

Abstract Ice clouds are an important component in precipitation systems. The radiative processes of ice clouds directly impact radiation in heat budget and the microphysical processes of ice clouds directly affect latent heat and net condensation through deposition processes, which may eventually change surface rainfall. Thus, torrential rainfall responses to radiative and microphysical processes of ice clouds during a landfall of severe tropical storm Bilis (2006) are investigated with the analysis of sensitivity experiments. The two-dimensional cloud-resolving model is integrated for 3 days with imposed zonally uniform vertical velocity, zonal wind, horizontal temperature and vapor advection from NCEP/GDAS data. One sensitivity experiment excludes the radiative effects of ice clouds and the other sensitivity experiment excludes ice microphysics and associated radiative and microphysical processes. Model domain mean surface rain rate is barely changed by the exclusion of radiative effects of ice clouds due to the small decrease in net condensation associated with the small reduction in latent heat as a result of the offset between the increase in radiative cooling and the decrease in heat divergence. The exclusion of microphysical effects of ice clouds decreases the mean rain rate simply through the suppression of latent heat as a result of the removal of deposition processes. The total exclusion of ice microphysics decreases the mean rain rate mainly through the exclusion of microphysical effects of ice clouds.

D. Wang (✉)
State Key Laboratory of Severe Weather (LaSW), Chinese Academy of Meteorological Sciences, Beijing, China
e-mail: d.wang@hotmail.com

D. Wang
Science System and Applications, Inc., Lanham, MD, USA

X. Li
NOAA/NESDIS/Center for Satellite Applications and Research, Camp Springs, MD, USA

W.-K. Tao
NASA/Goddard Space Flight Center, Greenbelt, MD, USA

1 Introduction

The landfall of typhoons over southeast coast of China leads to socio-economic losses as a result of major floods during Northern Hemisphere summer each year. Bilis, occurred in 2006, was a severe tropical storm that caused significant damage to areas of the Philippines, Taiwan, and southeastern China. It was the fifth tropical storm of the 2006 Pacific typhoon season recognized by the Joint Typhoon Warning Center. Despite never officially reaching typhoon strength, Bilis was responsible for $4.4 billion US dollars in damage and 672 fatalities in the Philippines, Taiwan area, and mainland China. Most of the damage was caused by widespread flash flooding and landslides associated with torrential rainfall. In particular, several sections of the Beijing–Guangzhou railway, a main rail route in China, were blocked by flooding and landslides, causing many delays and diversions. One train was surrounded by floodwaters in Lechang, Guangdong, and passengers had to be evacuated to a nearby school. At least 274 trains were affected and the train company refunded nearly 2 million tickets. After 3 days of repair work, the rail service resumed normal operations on July 18.

Wang D et al. (2009a, 2010) and Wang Y et al. (2010) employed a two-dimensional (2D) cloud-resolving model to conduct a simulation with imposed large-scale forcing from National Centers for Environmental Prediction (NCEP)/Global Data Assimilation System (GDAS) data. They

showed that the model domain mean surface rain rates on 15 and 16 July are similar, but they are contributed to mainly by stratiform rainfall on 15 July, and primarily by convective rainfall on 16 July, which result, respectively, from the imposed strong upward motions in the upper troposphere and weak downward motions in the lower troposphere on 15 July and upward motions throughout the troposphere on 16 July. Further, Wang et al. (2009b) carried out a sensitivity experiment by replacing vertically varying zonal winds with their mass-weighted means and found that the inclusion of negative vertical wind shear produces well-organized convection and strong convective rainfall since it leads to the conversion of kinetic energy from large-scale forcing to perturbation circulations.

The stratiform clouds that mainly contain ice hydrometeors are dominant in rainfall systems on 15 July and are the important ingredient of systems on 16 July. Thus, radiative and microphysical effects may impact cloud development and associated surface rainfall. The effects of ice clouds on the development of squall lines have been intensively studied with cloud-resolving model simulations (e.g., Yoshizaki 1986; Fovell and Ogura 1988; McCumber et al. 1991; Tao et al. 1991; Liu et al. 1997; Grabowski et al. 1999; Wu et al. 1999; Wu 2002; Li et al. 1999; Grabowski 2003; Gao et al. 2006). Ping et al. (2007) examined radiative and microphysical effects of ice clouds on rainfall in their equilibrium model simulations that are imposed by zero large-scale vertical velocity and revealed that the exclusion of radiative effects of ice clouds increases model domain mean surface rain rate by 43.1% whereas the removal of microphysical effects of ice clouds decreases the mean rain rate by 33.3%. Wang D et al. (2010) and Wang Y et al. (2010) analyzed microphysical and radiative effects of ice clouds on rainfall responses to the large-scale forcing during pre-summer heavy rainfall over southern China and found that microphysical and radiative effects of ice clouds impact the mean rain rate, depending on imposed large-scale forcing during different stages of entire life span of torrential rainfall event.

In this study, torrential rainfall responses to radiative and microphysical processes of ice clouds during the landfall of severe tropical storm Bilis (2006) are investigated by conducting and analyzing a series of sensitivity experiments. The model and sensitivity experiments are briefly described in the next section. The results are presented in Sect. 3. A summary is given in Sect. 4.

2 Model and sensitivity experiments

The model used in this study is the 2D version of the Goddard cumulus ensemble model (Sui et al. 1994, 1998) modified by Li et al. (1999). The cloud-resolving model was originally developed by Soong and Ogura (1980), Soong and Tao (1980), and Tao and Simpson (1993). The model includes prognostic equations for potential temperature, specific humidity, mixing ratios of cloud hydrometeors (cloud water, rain, cloud ice, snow, and graupel). The model has cloud microphysical parameterization schemes (Lin et al. 1983; Rutledge and Hobbs 1983, 1984; Tao et al. 1989; Krueger et al. 1995) and solar and thermal infrared radiation parameterization schemes (Chou et al. 1991, 1998; Chou and Suarez 1994). The model uses cyclic lateral boundary conditions, a horizontal domain of 768 km, a horizontal grid resolution of 1.5 km, and a time step of 12 s. The detailed model descriptions can be found in Gao and Li (2008a).

The reanalysis data from NCEP/GDAS that have a horizontal resolution of $0.5° \times 0.5°$ and a temporal resolution of 4 times per day are used to construct time-varied zonally uniform vertical velocity, zonal wind, and horizontal temperature and vapor advection. The forcing data are interpolated to be imposed in the model at each time step. The model is integrated from 0800 LST 14 July to 0800 LST 17 July 2006 (a total of 3 days) with the forcing averaged in a rectangular box of 108–116°E, 23–24°N (Fig. 1).

In addition to the control experiment (C) conducted by Wang et al. (2009a), two sensitivity experiments are conducted in this study. One sensitivity experiment excludes radiative effects of ice clouds by setting ice hydrometeor mixing ratio to zero in the calculations of radiation in CNIR, and the other sensitivity experiment totally removes ice microphysics and associated microphysical and radiative processes from the model in CNIM. The comparison between C and CNIR shows radiative effects of ice clouds on rainfall, the comparison between CNIR and CNIM reveals microphysical effects of ice clouds on rainfall in the absence of radiative effects of ice clouds, and the comparison between C and CNIM shows both radiative and microphysical effects of ice clouds on rainfall.

3 Results

Model domain mean surface rain rates are 2.685 mm h^{-1} in C and 2.731 mm h^{-1} in CNIR on 15 July, and 3.095 mm h^{-1} in C and 3.077 mm h^{-1} in CNIR on 16 July (Table 1); the mean surface rain rates are insensitive to radiative processes of ice clouds. The mean rain rates are decreased from 2.731 mm h^{-1} in CNIR to 2.151 mm h^{-1} in CNIM on 15 July and from 3.077 mm h^{-1} in CNIR to 2.845 mm h^{-1} in CNIM on 16 July. The decrease in the mean rain rate resulting from the exclusion of microphysical effects of ice clouds is larger on 15 July (21.2%) than on 16 July (7.5%). As a result, the total exclusion of ice

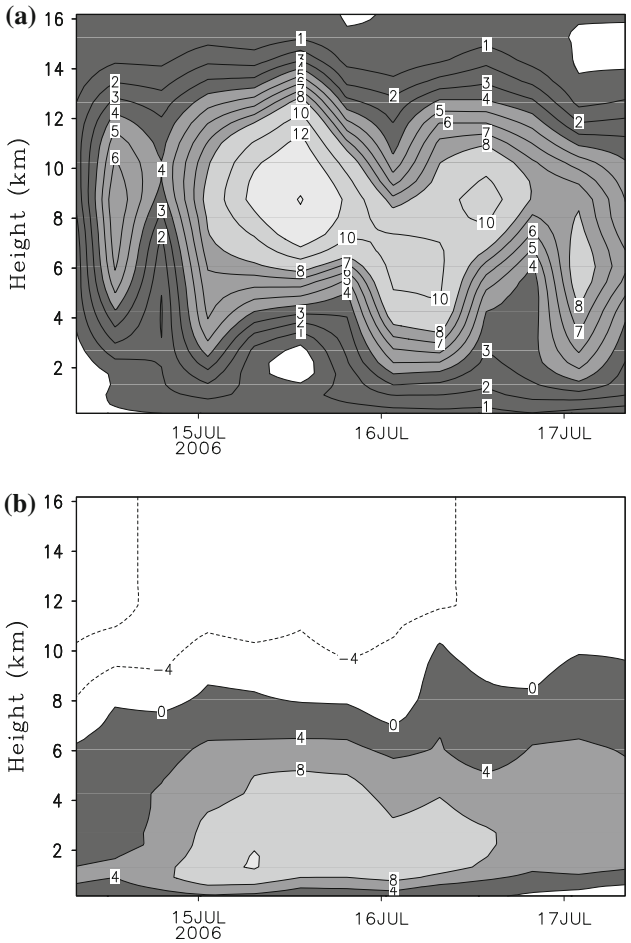

Fig. 1 Time–height distributions of **a** vertical velocity (cm s^{-1}) and **b** zonal wind (m s^{-1}) from 0800 LST 14 July–0800 LST 17 July 2006

microphysics (the exclusion of both radiative and microphysical effects of ice clouds) reduces the mean rain rates through the removal of microphysical effects of ice clouds.

To further elucidate torrential rainfall processes, surface rainfall budgets are analyzed. Following Gao et al. (2005) and Cui and Li (2006), surface rain rate (P_s) in the 2D framework can be written by

$$P_s = Q_{WVT} + Q_{WVF} + Q_{WVE} + Q_{CM}, \quad (1)$$

where

$$Q_{WVT} = -\frac{\partial[q_v]}{\partial t}, \quad (1a)$$

$$Q_{WVF} = -\left[\bar{u}^o\frac{\partial \bar{q}_v^o}{\partial x}\right] - \left[\bar{w}^o\frac{\partial \bar{q}_v}{\partial z}\right] - \left[\frac{\partial(u' q_v')}{\partial x}\right] - \left[\bar{u}^o\frac{\partial q_v'}{\partial x}\right] - \left[\bar{w}^o\frac{\partial q_v'}{\partial z}\right] - \left[w'\frac{\partial \bar{q}_v}{\partial z}\right], \quad (1b)$$

$$Q_{WVE} = E_s, \quad (1c)$$

Table 1 Daily and model domain means of surface rain rate (P_s), negative water vapor storage (Q_{WVT}), water vapor convergence (Q_{WVF}), surface evaporation (Q_{WVE}), and hydrometeor convergence and negative storage (Q_{CM}) in the control experiment (C), the experiment with the exclusion of ice radiative effects (CNIR), and the experiment with the total exclusion of ice microphysics (CNIM) and their differences for CNIR-C, CNIM–CNIR, and CNIM-C on (a) 15 July and (b) 16 July 2006

	C	CNIR	CNIM	CNIR-C	CNIM–CNIR	CNIM-C
(a)						
P_s	2.685	2.731	2.151	0.046	−0.580	−0.534
Q_{WVT}	−0.339	−0.271	−0.490	0.068	−0.219	−0.151
Q_{WVF}	2.913	2.902	2.865	−0.011	−0.037	−0.048
Q_{WVE}	0.037	0.039	0.034	0.002	−0.005	−0.003
Q_{CM}	0.073	0.060	−0.258	−0.013	−0.318	−0.331
(b)						
P_s	3.095	3.077	2.845	−0.018	−0.232	−0.250
Q_{WVT}	0.265	0.301	0.183	0.036	−0.118	−0.082
Q_{WVF}	2.726	2.725	2.672	−0.001	−0.053	−0.054
Q_{WVE}	0.001	0.001	0.000	0.000	−0.001	0.000
Q_{CM}	0.103	0.050	−0.010	−0.053	−0.060	−0.113

Unit is mm h^{-1}

$$Q_{CM} = -\frac{\partial[q_5]}{\partial t} - \left[\frac{\partial(uq_5)}{\partial x}\right]. \quad (1d)$$

Here, q_v is specific humidity; u and w are zonal and vertical wind components, respectively; E_s is surface evaporation rate; $q_5 = q_c + q_r + q_i + q_s + q_g$, q_c, q_r, q_i, q_s, q_g are the mixing ratios of cloud water, raindrops, cloud ice, snow, and graupel, respectively; Overbar denotes model domain mean; prime is a perturbation from domain mean; [ ] is a mass integration; and superscript ^{o} is an imposed observed value. The surface rain rate (P_s) is determined by negative water vapor storage (Q_{WVT}), water vapor convergence (Q_{WVF}), surface evaporation (Q_{WVE}), and hydrometeor convergence and negative storage (Q_{CM}).

In the control experiment, the mean rain rate corresponds primarily to the mean water vapor convergence rate (Table 1). Although the mean water vapor converge rate is higher on 15 July (2.913 mm h^{-1}) than on 16 July (2.726 mm h^{-1}), the mean local atmospheric moistening (−0.339 mm h^{-1}) occurs on 15 July whereas the mean local atmospheric drying (0.265 mm h^{-1}) appears on 16 July. As a result, the mean rain rate is lower on 15 July (2.685 mm h^{-1}) than on 16 July (3.095 mm h^{-1}). The mean water vapor convergence rates in CNIR are similar to those in C, which is responsible for insensitivity of the mean rain rate to radiative processes of ice clouds. The exclusion of radiative effects of ice clouds also slows down

the decrease of the mean local hydrometeor concentration from 0.073 mm h^{-1} in C to 0.060 mm h^{-1} in CNIR on 15 July and from 0.103 mm h^{-1} in C to 0.050 mm h^{-1} in CNIR on 16 July. The removal of radiative effects of ice clouds suppresses the mean local atmospheric moistening from −0.339 mm h^{-1} in C to −0.271 mm h^{-1} in CNIR on 15 July, whereas it enhances the mean local atmospheric drying from 0.265 into 0.301 mm h^{-1} in CNIR on 16 July. While the mean water vapor convergence rates in CNIM are similar to those in CNIR, the decreases in the mean rain rate resulting from the exclusion of microphysical effects of ice clouds are primarily associated with the mean local hydrometeor change from decrease in CNIR (0.060 mm h^{-1}) to increase in CNIM (−0.258 mm h^{-1}) and the increase in the mean local atmospheric moistening from −0.271 mm h^{-1} in CNIR to −0.490 mm h^{-1} in CNIM on 15 July and the decrease in the mean local atmospheric drying from 0.301 mm h^{-1} in CNIR to 0.183 mm h^{-1} in CNIM on 16 July.

The change of Q_{CM} in three experiments impacts the mean rain rate. Thus, Q_{CM} is further broken down into

$$Q_{CM} = Q_{CMC} + Q_{CMR} + Q_{CMI} + Q_{CMS} + Q_{CMG}, \quad (2)$$

where

$$Q_{CMC} = -\frac{\partial[q_c]}{\partial t} - \left[\frac{\partial}{\partial x}(\bar{u}^o + u')q_c\right], \quad (2a)$$

$$Q_{CMR} = -\frac{\partial[q_r]}{\partial t} - \left[\frac{\partial}{\partial x}(\bar{u}^o + u')q_r\right], \quad (2b)$$

$$Q_{CMI} = -\frac{\partial[q_i]}{\partial t} - \left[\frac{\partial}{\partial x}(\bar{u}^o + u')q_i\right], \quad (2c)$$

$$Q_{CMS} = -\frac{\partial[q_s]}{\partial t} - \left[\frac{\partial}{\partial x}(\bar{u}^o + u')q_s\right], \quad (2d)$$

$$Q_{CMG} = -\frac{\partial[q_g]}{\partial t} - \left[\frac{\partial}{\partial x}\left(\bar{u}^o + u'\right)q_g\right]. \quad (2e)$$

Here, Q_{CMC}, Q_{CMR}, Q_{CMI}, Q_{CMS}, and Q_{CMG} are hydrometeor convergence and negative storage from cloud water, rain, cloud ice, snow, and graupel, respectively. The slowdown in the decrease of the mean local hydrometeor concentration from the exclusion of radiative effects of ice clouds is associated with the slowdown in the decrease of the mean local rain hydrometeor from 0.112 mm h^{-1} in C to 0.090 mm h^{-1} in CNIR and the enhancement in the increase of the mean local ice hydrometeor (the sum of cloud ice, snow, and graupel hydrometeors) from −0.019 mm h^{-1} in C to −0.037 mm h^{-1} in CNIR on 15 July, whereas it is related to the mean local ice hydrometeor concentration from decrease in C (0.022 mm h^{-1}) to increase in CNIR (−0.062 mm h^{-1}) on 16 July (Table 2). The mean local hydrometeor change from decrease in CNIR to increase in CNIM resulting from the exclusion of microphysical effects of ice clouds is primarily from cloud water hydrometeor (−0.313 mm h^{-1} on 15 July and −0.107 mm h^{-1} on 16 July for CNIM–CNIR). The large increase of cloud water hydrometeor in CNIM is consistent with the results in the sensitivity experiment with the total removal of ice microphysics during TOGA COARE when the vapor condensation cannot be consumed by the collection of cloud water by rain and the autoconversion of cloud water to rain (Gao et al. 2006). With the total exclusion of ice microphysics, the model produces the large increase of cloud water hydrometeor concentration, which leads to the decrease of the mean rain rate in CNIM.

The radiative processes of ice clouds directly impact the radiation term in heat budget, whereas the microphysical processes of ice clouds directly affect the latent heat in heat budget and the net condensation in cloud and water vapor

Table 2 Breakdown of daily and model domain means of Q_{CM} to Q_{CMC}, Q_{CMR}, $Q_{CMI} + Q_{CMS} + Q_{CMG}$ in the control experiment (C), the experiment with the exclusion of ice radiative effects (CNIR), and the experiment with the total exclusion of ice microphysics (CNIM) and their differences for CNIR-C, CNIM–CNIR, and CNIM-C on (a) 15 July and (b) 16 July 2006

	C	CNIR	CNIM	CNIR-C	CNIM–CNIR	CNIM-C
(a)						
Q_{CM}	0.073	0.060	−0.258	−0.013	−0.318	−0.331
Q_{CMC}	−0.020	0.007	−0.306	0.027	−0.313	−0.286
Q_{CMR}	0.112	0.090	0.048	−0.022	−0.042	−0.064
$Q_{CMI} + Q_{CMS} + Q_{CMG}$	−0.019	−0.037	0.000	−0.018	0.037	0.019
(b)						
Q_{CM}	0.103	0.050	−0.010	−0.053	−0.060	−0.113
Q_{CMC}	−0.011	0.013	−0.094	0.024	−0.107	−0.083
Q_{CMR}	0.092	0.099	0.084	0.007	−0.015	−0.008
$Q_{CMI} + Q_{CMS} + Q_{CMG}$	0.022	−0.062	0.000	−0.084	0.062	−0.022

Unit is mm h^{-1}

budgets. Thus the mean heat budgets in the three experiments are analyzed. Following Gao and Li (2008b), the mean heat budget can be expressed as

$$S_{\mathrm{HT}} + S_{\mathrm{HF}} + S_{\mathrm{HS}} + S_{\mathrm{LH}} + S_{\mathrm{RAD}} = 0, \tag{3}$$

where

$$S_{\mathrm{HT}} = -\frac{\partial\langle\overline{T}\rangle}{\partial t}, \tag{3a}$$

$$S_{\mathrm{HF}} = -\left\langle \bar{u}^{\mathrm{o}}\frac{\partial\overline{T}^{\mathrm{o}}}{\partial x}\right\rangle - \left\langle \pi\bar{w}^{\mathrm{o}}\frac{\partial\bar{\theta}}{\partial z}\right\rangle, \tag{3b}$$

$$S_{\mathrm{HS}} = \overline{H}_{\mathrm{s}}, \tag{3c}$$

$$S_{\mathrm{LH}} = \frac{1}{c_{\mathrm{p}}}\langle\overline{Q}_{\mathrm{cn}}\rangle, \tag{3d}$$

$$S_{\mathrm{RAD}} = \frac{1}{c_{\mathrm{p}}}\langle\overline{Q}_{\mathrm{R}}\rangle. \tag{3e}$$

Here, S_{HT}, S_{HF}, S_{HS}, S_{LH}, and S_{RAD} are negative heat storage, heat convergence, surface sensible heat, latent heat, and radiative heating/cooling, respectively; T and θ are air temperature and potential temperature, respectively. $\pi = (p/p_{\mathrm{o}})^{\kappa}$, $\kappa = R/c_{\mathrm{p}}$, R is the gas constant, c_{p} is the specific heat of dry air at constant pressure p, and $p_{\mathrm{o}} = 1{,}000$ hPa. $\overline{H}_{\mathrm{s}}$ is surface sensible heat flux, Q_{cn} is the condensation heating, Q_{R} is the net radiative heating due to solar heating and infrared cooling. $\langle()\rangle\left(=\int_{z_b}^{z_t}\bar{\rho}()\mathrm{d}z/\int_{z_b}^{z_t}\bar{\rho}\mathrm{d}z\right)$ is mass-weighted mean.

The increase in the mean radiative cooling (-0.031°C h^{-1} for CNIR-C) from the exclusion of radiative effects of ice clouds is largely balanced by the decrease in the mean heat divergence (0.23°C h^{-1} for CNIR-C) on 15 July, whereas the increase in the mean radiative cooling (-0.021°C h^{-1} for CNIR-C) is largely offset by the decrease in mean heat divergence (0.008°C h^{-1} for CNIR-C) and the increase in the mean local atmospheric cooling (0.009°C h^{-1} for CNIR-C) on 16 July (Table 3). As a result, the increases in the mean latent heating are small. The increase in the mean latent heat corresponds to the enhanced mean radiative cooling resulting from the exclusion of radiative effects of ice clouds. From the mean cloud budget, the mean net condensation can be calculated by $P_{\mathrm{s}} - Q_{\mathrm{CM}}$ (e.g., Gao and Li 2008b). The increase in the mean net condensation (0.059 mm h^{-1} on 15 July and 0.035 mm h^{-1} on 16 July for CNIR-C calculated from Table 1) is associated with the increase in the mean latent heat. The increase in the net condensation leads to the increase in the mean rain rate (0.046 mm h^{-1} for CNIR-C) on 15 July, whereas it changes the mean local hydrometeor concentration from decrease in C to increase in CNIR, which decreases the mean rain rate (-0.018 mm h^{-1} for CNIR-C) (Table 1).

Table 3 Daily and model domain means of radiative heating (S_{RAD}), negative heat storage (S_{HT}), heat convergence (S_{HF}), surface sensible flux (S_{HS}), and latent heat (S_{LH}) in the control experiment (C), the experiment with the exclusion of ice radiative effects (CNIR), and the experiment with the total exclusion of ice microphysics (CNIM) and their differences for CNIR-C, CNIM–CNIR, and CNIM-C on (a) 15 July and (b) 16 July 2006

	C	CNIR	CNIM	CNIR-C	CNIM–CNIR	CNIM-C
(a)						
S_{RAD}	−0.012	−0.043	−0.025	−0.031	0.018	−0.013
S_{HT}	0.162	0.160	0.152	−0.002	−0.008	−0.010
S_{HF}	−0.821	−0.798	−0.756	0.023	0.042	0.065
S_{HS}	0.004	0.004	0.003	0.000	−0.001	−0.001
S_{LH}	0.667	0.677	0.626	0.010	−0.051	−0.041
(b)						
S_{RAD}	−0.036	−0.057	−0.040	−0.021	0.017	−0.004
S_{HT}	0.139	0.148	0.137	0.009	−0.011	−0.002
S_{HF}	−0.882	−0.874	−0.847	0.008	0.027	0.035
S_{HS}	0.000	0.000	0.000	0.000	0.000	0.000
S_{LH}	0.780	0.784	0.749	0.004	−0.035	−0.031

Unit is °C h^{-1}

Thus, the offset between the enhanced mean radiative cooling from the exclusion of radiative effects of ice clouds and weakened mean heat divergence is responsible for the insensitivity of the mean rain rate to radiative effects of ice clouds.

The removal of microphysical effects of ice clouds cuts deposition processes and thus reduces associated mean latent heating (-0.051°C h^{-1} on 15 July and -0.035°C h^{-1} on 16 July for CNIM–CNIR; Table 3) and mean net condensation (-0.262 mm h^{-1} on 15 July and -0.172 mm h^{-1} on 16 July for CNIM–CNIR calculated from Table 1). As a result, the mean rain rates are decreased (-0.580 mm h^{-1} on 15 July and -0.232 mm h^{-1} on 16 July for CNIM–CNIR; Table 1).

Model domain mean surface rain rate is from convective and stratiform regions. Thus, the convective-stratiform rainfall partitioning method developed by Tao et al. (1993) and modified by Sui et al. (1994) are used in this study. In the partitioning scheme, model grid points in the surface rain field that have a rain rate twice as large as the average taken over the surrounding four grid points (2 neighbors on each side) are identified as the cores of convective cells. For each core grid point, the grid point on either side is also considered convective. In addition, any grid point with a rain rate of 20 mm h^{-1} or more is designated as convective regardless of the above criteria. Further, the point is made convective if the cloud water and ice or the updraft exceeds certain threshold values. All nonconvective cloudy points are further regarded as stratiform.

The exclusion of radiative effects of ice clouds decreases stratiform rain from 2.156 mm h^{-1} in C to 2.093 mm h^{-1} in CNIR on 15 July and from 1.106 mm h^{-1} in C to 0.993 mm h^{-1} in CNIR on 16 July (Table 4). The small decrease in stratiform rainfall on 15 July is associated with the balance between the decreases in water vapor convergence (−0.296 mm h^{-1} for CNIR-C) and local atmospheric moistening (0.128 mm h^{-1} for CNIR-C) over raining stratiform regions and the increase in hydrometeor loss/convergence (0.101 mm h^{-1} for CNIR-C). The decrease in stratiform rainfall on 16 July is primarily associated with the significant decrease in water vapor convergence over raining stratiform regions (−0.480 mm h^{-1} for CNIR-C). The exclusion of microphysical effects of ice clouds decreases stratiform rain rate from 2.093 mm h^{-1} in CNIR to 1.682 mm h^{-1} in CNIM on 15 July, whereas it increases stratiform rain rate from 0.993 mm h^{-1} in CNIR to 1.182 mm h^{-1} in CNIM on 16 July. The decrease in stratiform rainfall corresponds primarily to the change from hydrometeor loss/convergence in CNIR (0.182 mm h^{-1}) to hydrometeor gain/divergence in CNIM (−0.052 mm h^{-1}) on 15 July, whereas the increase in stratiform rainfall corresponds to the increase in water vapor convergence (0.764 mm h^{-1} for CNIM–CNIR) over raining stratiform regions on 16 July. The decrease in stratiform rainfall resulting from the total exclusion of ice microphysics is primarily related to the decrease in water vapor convergence (−0.380 mm h^{-1} for CNIM-C) over raining stratiform regions on 15 July, whereas the increase in stratiform rainfall corresponds to the hydrometeor change from loss/convergence in CNIR (0.262 mm h^{-1}) to gain/divergence in CNIM (−0.074 mm h^{-1}) on 16 July.

The exclusion of radiative effects of ice clouds increases convective rain rates from 0.528 mm h^{-1} in C to 0.638 mm h^{-1} in CNIR on 15 July and from 1.990 mm h^{-1} in C to 2.084 mm h^{-1} in CNIR on 16 July, which are associated with the increases in water vapor convergence over convective regions (0.295 mm h^{-1} on 15 July and 0.425 mm h^{-1} on 16 July for CNIR-C) (Table 5). The removal of microphysical effects of ice clouds decreases convective rain rates from 0.638 mm h^{-1} in CNIR to 0.469 mm h^{-1} in CNIM on 15 July and from 2.084 mm h^{-1} in CNIR to 1.663 mm h^{-1} in CNIM on 16 July, which are primarily related to the decreases in water vapor convergence over convective regions (−0.168 mm h^{-1} on 15 July and −0.751 mm h^{-1} on 16 July for CNIM–CNIR). The total exclusion of ice microphysics decreases convective rain rate by 11.2% on 15 July (−0.059 mm h^{-1} for CNIM–CNIR) and 16.4% on 16 July (−0.327 mm h^{-1} for CNIM–CNIR). The decreases in convective rain rate resulting from the total exclusion of ice microphysics are associated with the decrease in local atmospheric drying over convective regions (−0.099 mm h^{-1} for CNIM–CNIR) and the hydrometeor change from loss/convergence in C (0.005 mm h^{-1}) and gain/divergence in CNIM (−0.084 mm h^{-1}) on 15 July and the decreases in local

Table 4 Daily means of surface rain rate (P_s), negative water vapor storage (Q_{WVT}), water vapor convergence (Q_{WVF}), surface evaporation (Q_{WVE}), and hydrometeor convergence and negative storage (Q_{CM}) over raining stratiform regions in the control experiment (C), the experiment with the exclusion of ice radiative effects (CNIR), and the experiment with the total exclusion of ice microphysics (CNIM) and their differences for CNIR-C, CNIM–CNIR, and CNIM-C on (a) 15 July and (b) 16 July 2006

	C	CNIR	CNIM	CNIR-C	CNIM–CNIR	CNIM-C
(a)						
P_s	2.156	2.093	1.682	−0.063	−0.411	−0.474
Q_{WVT}	−0.424	−0.296	−0.377	0.128	−0.081	0.047
Q_{WVF}	2.469	2.173	2.089	−0.296	−0.084	−0.380
Q_{WVE}	0.031	0.034	0.021	0.003	−0.013	−0.010
Q_{CM}	0.081	0.182	−0.052	0.101	−0.234	−0.133
(b)						
P_s	1.106	0.993	1.182	−0.113	0.189	−0.076
Q_{WVT}	−0.252	−0.035	−0.124	0.217	−0.089	0.128
Q_{WVF}	1.095	0.615	1.379	−0.480	0.764	0.284
Q_{WVE}	0.001	0.001	0.000	0.000	−0.001	−0.001
Q_{CM}	0.262	0.412	−0.074	0.150	−0.486	−0.336

Unit is mm h^{-1}

Table 5 Daily means of surface rain rate (P_s), negative water vapor storage (Q_{WVT}), water vapor convergence (Q_{WVF}), surface evaporation (Q_{WVE}), and hydrometeor convergence and negative storage (Q_{CM}) over convective regions in the control experiment (C), the experiment with the exclusion of ice radiative effects (CNIR), and the experiment with the total exclusion of ice microphysics (CNIM) and their differences for CNIR-C, CNIM–CNIR, and CNIM-C on (a) 15 July and (b) 16 July 2006

	C	CNIR	CNIM	CNIR-C	CNIM–CNIR	CNIM-C
(a)						
P_s	0.528	0.638	0.469	0.110	−0.169	−0.059
Q_{WVT}	0.137	0.069	0.038	−0.068	−0.031	−0.099
Q_{WVF}	0.383	0.678	0.510	0.295	−0.168	0.127
Q_{WVE}	0.003	0.002	0.006	−0.001	0.005	0.003
Q_{CM}	0.005	−0.111	−0.084	−0.116	0.027	−0.089
(b)						
P_s	1.990	2.084	1.663	0.094	−0.421	−0.327
Q_{WVT}	0.487	0.371	0.252	−0.116	−0.119	−0.235
Q_{WVF}	1.665	2.090	1.339	0.425	−0.751	−0.326
Q_{WVE}	0.000	0.000	0.000	0.000	0.000	0.000
Q_{CM}	−0.162	−0.378	0.073	−0.216	0.451	0.235

Unit is mm h^{-1}

atmospheric drying (-0.235 mm h^{-1} for CNIM–CNIR) and water vapor convergence (-0.326 mm h^{-1} for CNIM–CNIR) over convective regions on 16 July.

4 Summary

Torrential rainfall responses to radiative and microphysical processes of ice clouds during a landfall of severe tropical storm Bilis (2006) is investigated analyzing a series of sensitivity experiments. The experiments are conducted with a 2D cloud-resolving model. The model is integrated for 3 days with imposed zonally uniform vertical velocity, zonal wind, horizontal temperature and vapor advection from NCEP/GDAS data. One sensitivity experiment excludes radiative effects of ice clouds by setting mixing ratios of ice hydrometeors (cloud ice, snow, and graupel) to zero in the calculations of radiation whereas the other sensitivity experiment excludes ice microphysics and associated ice microphysical and radiative processes. The analysis is conducted on 15 and 16 July during the torrential rainfall event. The major results include

- Model domain mean surface rain rate is insensitive to radiative effects of ice clouds. The mean heat budgets show that the increase in infrared radiative cooling resulting from the exclusion of radiative effects of ice clouds is largely offset by the decrease in heat divergence, which leads to the small increase in latent heat and associated net condensation. Ping et al. (2007) showed the removal of radiative effects of ice clouds increases the mean rain rate by 43.1% since the increase in the mean latent heat corresponds to the increase in infrared radiative cooling in the absence of the mean heat divergence in the equilibrium model experiments with imposed zero large-scale vertical velocity. This suggests that the variation of heat divergence associated with upward motions plays an important role in determining the responses of latent heat to the variation of infrared radiative cooling in the heat balance when radiative effects of ice clouds turn off.
- The exclusion of microphysical effects of ice clouds significantly decreases the mean latent heat. The decrease in latent heat from the removal of microphysical effects of ice clouds is larger on 15 July than on 16 July since the dominate stratiform clouds and rainfall are associated with imposed large-scale forcing of strong upward motions in the upper motions and weak downward motions in the lower troposphere on 15 July and strong growth of convective clouds and rainfall is related to the extension of imposed large-scale upward motions to the lower troposphere on 16 July. As a result, the decrease in the mean rain rate is larger on 15 July (21.2%) than on 16 July (7.5%).
- Although the radiative processes of ice clouds does not impact the mean rain rate, it increases convective rain rate by enhancing water vapor convergence over convective regions and decreases stratiform rain rate by suppressing water vapor convergence over raining stratiform regions. The decreases in the mean rainfall from the exclusion of microphysical effects of ice clouds are mainly from raining stratiform regions on 15 July where the hydrometeor loss/convergence is changed into the hydrometeor gain/divergence and from convective regions on 16 July in which the water vapor convergence is suppressed.

Acknowledgments The authors thank two anonymous reviewers for their constructive comments. This research was supported by the State Key Basic Research Development Program (2009CB421504), and the National Natural Science Foundation under the Grant No. 40633016, 40875022 and 40830958.

References

Chou M-D, Suarez MJ (1994) An efficient thermal infrared radiation parameterization for use in general circulation model, vol 3. NASA Tech. Memo. 104606, 85 pp (available from NASA/Goddard Space Flight Center, Code 913, Greenbelt, MD 20771)

Chou M-D, Kratz DP, Ridgway W (1991) Infrared radiation parameterization in numerical climate models. J Clim 4:424–437

Chou M-D, Suarez MJ, Ho C-H, Yan MM-H, Lee K-T (1998) Parameterizations for cloud overlapping and shortwave single scattering properties for use in general circulation and cloud ensemble models. J Atmos Sci 55:201–214

Cui X, Li X (2006) Role of surface evaporation in surface rainfall processes. J Geophys Res 111:D17112. doi:10.1029/2005JD006876

Fovell RG, Ogura Y (1988) Numerical simulation of a midlatitude squall line in two dimensions. J Atmos Sci 45:3846–3879

Gao S, Li X (2008a) Cloud-resolving modeling of convective processes. Springer, Dordrecht, 206 pp

Gao S, Li X (2008b) Responses of tropical deep convective precipitation systems and their associated convective and stratiform regions to the large-scale forcing. Q J R Meteorol Soc 134:2127–2141

Gao S, Cui X, Zhu Y, Li X (2005) Surface rainfall processes as simulated in a cloud resolving model. J Geophys Res 110:D10202. doi:10.1029/2004JD005467

Gao S, Ran L, Li X (2006) Impacts of ice microphysics on rainfall and thermodynamic processes in the tropical deep convective regime: a 2D cloud-resolving modeling study. Mon Weather Rev 134:3015–3024

Grabowski WW (2003) Impact of ice microphysics on multiscale organization of tropical convection in two-dimensional cloud-resolving simulations. Q J R Meteorol Soc 129:67–81

Grabowski WW, Wu X, Moncrieff MW (1999) Cloud-resolving model of tropical cloud systems during Phase III of GATE. Part III: effects of cloud microphysics. J Atmos Sci 56:2384–2402

Krueger SK, Fu Q, Liou KN, Chin H-NS (1995) Improvement of an ice-phase microphysics parameterization for use in numerical simulations of tropical convection. J Appl Meteorol 34:281–287

Li X, Sui C-H, Lau K-M, Chou M-D (1999) Large-scale forcing and cloud-radiation interaction in the tropical deep convective regime. J Atmos Sci 56:3028–3042

Lin Y-L, Farley RD, Orville HD (1983) Bulk parameterization of the snow field in a cloud model. J Clim Appl Meteorol 22:1065–1092

Liu C, Moncrieff MW, Zipser EJ (1997) Dynamic influence of microphysics in tropical squall lines: a numerical study. Mon Weather Rev 125:2193–2210

McCumber M, Tao W-K, Simpson J, Penc R, Soong S-T (1991) Comparison of ice-phase microphysical parameterization schemes using numerical simulations of tropical convection. J Appl Meteorol 30:985–1004

Ping F, Luo Z, Li X (2007) Microphysical and radiative effects of ice clouds on tropical equilibrium states: a two-dimensional cloud-resolving modeling study. Mon Weather Rev 135:2794–2802

Rutledge SA, Hobbs PV (1983) The mesoscale and microscale structure and organization of clouds and precipitation in midlatitude cyclones. Part VIII: a model for the "seeder-feeder" process in warm-frontal rainbands. J Atmos Sci 40:1185–1206

Rutledge SA, Hobbs PV (1984) The mesoscale and microscale structure and organization of clouds and precipitation in midlatitude cyclones. Part XII: a diagnostic modeling study of precipitation development in narrow cold-frontal rainbands. J Atmos Sci 41:2949–2972

Soong ST, Ogura Y (1980) Response of tradewind cumuli to large-scale processes. J Atmos Sci 37:2035–2050

Soong ST, Tao W-K (1980) Response of deep tropical cumulus clouds to mesoscale processes. J Atmos Sci 37:2016–2034

Sui C-H, Lau K-M, Tao W-K, Simpson J (1994) The tropical water and energy cycles in a cumulus ensemble model. Part I: equilibrium climate. J Atmos Sci 51:711–728

Sui C-H, Li X, Lau K-M (1998) Radiative-convective processes in simulated diurnal variations of tropical oceanic convection. J Atmos Sci 55:2345–2359

Tao W-K, Simpson J (1993) The Goddard cumulus ensemble model. Part I: model description. Terr Atmos Ocean Sci 4:35–72

Tao W-K, Simpson J, McCumber M (1989) An ice-water saturation adjustment. Mon Weather Rev 117:231–235

Tao W-K, Simpson J, Soong S-T (1991) Numerical simulation of a subtropical squall line over the Taiwan Strait. Mon Weather Rev 119:2699–2723

Tao W-K, Simpson J, Sui C-H, Ferrier B, Lang S, Scala J, Chou M-D, Pickering K (1993) Heating, moisture, and water budgets of tropical and midlatitude squall lines: comparisons and sensitivity to longwave radiation. J Atmos Sci 50:673–690

Wang D, Li X, Tao W-K, Liu Y, Zhou H (2009a) Torrential rainfall processes associated with a landfall of severe tropical strom Bilis (2006): a two-dimensional cloud-resolving modeling study. Atmos Res 91:94–104

Wang D, Li X, Tao W-K, Wang Y (2009b) Effects of vertical wind shear on convective development during a landfall of severe tropical storm Bilis (2006). Atmos Res 94:270–275

Wang D, Li X, Tao W-K (2010) Responses of vertical structures in convective, stratiform regions to large-scale forcing during the landfall of severe tropical storm Bilis (2006). Adv Atmos Sci 27:33–46

Wang Y, Shen X, Li X (2010) Microphysical and radiative effects of ice clouds on responses of rainfall to the large-scale forcing during pre-summer heavy rainfall over southern China. Atmos Res 97:35–46

Wu X (2002) Effects of ice microphysics on tropical radiative-convective-oceanic quasi-equilibrium states. J Atmos Sci 59:1885–1897

Wu X, Hall WD, Grabowski WW, Moncrieff MW, Collins WD, Kiehl JT (1999) Long-term behavior of cloud systems in TOGA COARE and their interactions with radiative and surface processes. Part II: effects of ice microphysics on cloud-radiation interaction. J Atmos Sci 56:3177–3195

Yoshizaki M (1986) Numerical simulations of tropical squall-line clusters: two-dimensional model. J Meteorol Soc Jpn 64:469–491